PCCP

PAPER

View Article Online
View Journal | View Issue

Cite this: *Phys. Chem. Chem. Phys.*, 2014, **16**, 18163

Correction of erroneously packed protein's side chains in the NMR structure based on *ab initio* chemical shift calculations†

Tong Zhu,[a] John Z. H. Zhang[ab] and Xiao He*[ab]

Received 10th June 2014,
Accepted 15th July 2014

DOI: 10.1039/c4cp02553a

www.rsc.org/pccp

In this work, protein side chain ^{1}H chemical shifts are used as probes to detect and correct side-chain packing errors in protein's NMR structures through structural refinement. By applying the automated fragmentation quantum mechanics/molecular mechanics (AF-QM/MM) method for *ab initio* calculation of chemical shifts, incorrect side chain packing was detected in the NMR structures of the Pin1 WW domain. The NMR structure is then refined by using molecular dynamics simulation and the polarized protein-specific charge (PPC) model. The computationally refined structure of the Pin1 WW domain is in excellent agreement with the corresponding X-ray structure. In particular, the use of the PPC model yields a more accurate structure than that using the standard (nonpolarizable) force field. For comparison, some of the widely used empirical models for chemical shift calculations are unable to correctly describe the relationship between the particular proton chemical shift and protein structures. The AF-QM/MM method can be used as a powerful tool for protein NMR structure validation and structural flaw detection.

Introduction

Over the past 20 years, nuclear magnetic resonance (NMR) spectroscopy has emerged as a powerful and widely used technique for studying the structure and dynamics of bio-molecules.[1,2] To date, more than 8000 NMR protein structures have been deposited into the Protein Data Bank (PDB) with increase in the structural size. Unlike X-ray crystallography, NMR spectroscopy cannot measure the atomic positions of the protein directly. The measured experimental NMR data are used as structural constraints in several computational methods to determine protein three-dimensional conformation. Standard NMR experiments consist of several stages: data recording, spectra assignment, structure calculation and validation.[3,4] Although more experimental constraints such as heteronuclear *J*-couplings and residual dipolar coupling have been included in the structure determination step in recent years, NOE signals still play an important role in protein NMR structure determination.[5] However, as the protein size increases, NOEs become progressively less useful because they are very difficult to measure and error-prone.[6]

Recently, some NMR researchers have been searching for ways to skip the NOE step and to use the chemical shifts to determine the protein 3D structures.[7–9] It has been demonstrated that reasonably accurate protein structures can be determined directly from chemical shifts by several groups.[10–21] Chemical shifts are easy to measure and are the most accurate measurable NMR parameters. In addition, they are highly sensitive to the local structure of proteins, and reflect a number of specific features of protein conformations including secondary structure, hydrogen bonding and the proximity to aromatic rings. However, a detailed relationship between the protein structure and the corresponding chemical shifts is still not very clear, and the stereo-specific assignment also increases the complexity. Most of the widely used protein chemical shift predictors mainly focus on predicting backbone chemical shifts. To the best of our knowledge, only four empirical models can predict all possible side chain chemical shifts (SHIFTX2,[22] PROSHIFT,[23] SHIFTS4.1[24–26] and SHIFTCALC[27–31]). Since backbone chemical shifts are more sensitive to the conformation of peptide moieties, they reflect the detailed information of the secondary structure, backbone dihedral angles, hydrogen bonds and dynamics. In contrast, side-chain chemical shifts (especially the ^{1}H ones) are very sensitive to the interactions between

[a] *State Key Laboratory of Precision Spectroscopy, Institute of Theoretical and Computational Science, East China Normal University, Shanghai, 200062, China. E-mail: xiaohe@phy.ecnu.edu.cn*

[b] *NYU-ECNU Center for Computational Chemistry at NYU Shanghai, Shanghai, 200062, China*

† Electronic supplementary information (ESI) available: Fig. S1 shows hydrogen bond probabilities of several important hydrogen bonds in the Pin1 WW domain during MD simulations using the Amber ff99SB and PPC charge models. Fig. S2 demonstrates the number of hydrogen bonds in the Pin1 WW domain as a function of MD simulation time for both Amber ff99SB and PPC trajectories. See DOI: 10.1039/c4cp02553a

spatially adjacent atoms, especially to the influence of ring current effects, hydrogen bonding and electrostatic interactions, so they accurately reflect the fine details of the protein tertiary structure. Hence, to predict protein structures based on chemical shifts, the chemical shifts of side-chain atoms should also be included.[3,32] In a previous study by Vendruscolo and co-workers, they found that the quality of protein structures can be readily validated using the side-chain NMR chemical shifts.[3]

However, as the essential factors governing the side-chain chemical shifts are complicated, neither the structure-based nor the sequence-based empirical methods are capable of providing accurate predictions. Recently, quantum chemical methods have become increasingly useful for protein NMR chemical shift calculations, as they allow one to investigate structural and environmental effects in a systematic and controlled manner[33] and do not need any knowledge based information or additional NMR data.[34–43] In our previous studies, a recently developed automated fragmentation quantum mechanics/molecular mechanics (AF-QM/MM) approach was used to calculate NMR chemical shifts for proteins, and the solvent effects were also included by using both the Poisson–Boltzmann (PB) model and explicit water molecules.[34–36] The AF-QM/MM-PB method has been demonstrated to give results in excellent agreement with those from full quantum calculations, and the computed chemical shifts have very good correlation with the experimental values. In this study, we explore the ability of AF-QM/MM-PB calculated chemical shifts to validate the Pin1 WW domain NMR structures and further aid the protein structure refinement process by combining with polarized protein-specific charges (PPC).

Methods

A. Chemical shift calculations using the AF-QM/MM-PB approach

In this work, the protein chemical shifts are calculated by the linear-scaling AF-QM/MM-PB method. In this approach, the entire protein is divided into non-overlapping fragments termed core regions. The residues within a certain range from the core region are included in the buffer region. Both the core and the buffer regions are treated by quantum mechanics, while the remainder of the protein is described using an empirical point-charge model to account for the electrostatic effect. The surface charges distributed on the protein surface calculated using the Poisson–Boltzmann (PB) model were used to mimic the solvation effects. Each core-centric (core + buffer) QM/MM calculation is carried out separately, and only the shielding constants of the atoms in the core region are extracted from individual QM/MM calculations. The details of partitioning the system and the definition of the buffer region are described in our previous studies.[34–36] NMR calculation for each fragment is performed by the GIAO method using the Gaussian 09 program[44] at the B3LYP/6-31G** level. The calculated results are referenced to the isotropic shielding constants computed for tetramethylsilane (TMS) at the same level of theory in the gas phase. All the fragment calculations were performed in parallel on a Linux cluster with 12-Core Intel Xeon 3.0 GHz processors. The calculation for each fragment takes about 1–3 hours of computer time on a single node using the current definition of the buffer region.

B. Structure refinement using simulated annealing and molecular dynamics (MD) simulation

The coordinates and restraint data for the Pin1 WW domain were retrieved from the PDB website using the PDB id of 1I6C[45] and BMRB id of 4882. Of the ten conformers contained in the PDB file, only the first was used in simulations. Flat-well distance restraints weighted at 50 kcal mol^{-1} $Å^{-2}$ were added within 0.5 Å of the bounds of NOE data. For the sake of convenience, the IUPAC nomenclature was used.[46] All MD simulations were performed using the AMBER12 software suite[47] with the Amber ff99SB force field. The protein was placed in a periodic rectangular box of TIP3P water molecules. The distance from the surface of the box to the closest atom of the solute was set to 10 Å. Counter ions were added to neutralize the system. The entire system was first energy minimized using the steepest descent method followed by conjugate gradient minimization. The system is then heated from 0 to 300 K over 100 ps. After heating, the system underwent several steps of heating and annealing between 10 K and 600 K over 300 ps. Finally, a 5 ns production simulation was performed at constant pressure (in the NPT ensemble). During the first 2.5 ns of the production run, the NOE restraints were added. In addition, our previous studies[48] have found that MD simulations using the standard nonpolarizable Amber force field may break some of the backbone hydrogen bonds in native secondary structures, which results in structural deformation due to the lack of electronic polarization effects. Therefore, in this study, we also employed the recently developed polarized protein-specific charge (PPC) model to provide a new set of atomic charges for a better description of the protein dynamics.[49] The PPC charges were fitted at the B3LYP/6-31G** level based on the optimized protein structure using the Amber ff99SB force field. The detailed description of this method can be found in our previous paper.[49] To make a direct comparison with the Amber ff99SB force field, MD simulation was also performed using the PPC model. In the simulation using PPC, the atomic charges of the Amber ff99SB force field were simply replaced by PPC, which were updated every 500 ps during the MD simulation, while the rest of the ff99SB force field parameters were retained.

Results and discussion

Since chemical shifts are very sensitive to specific structural features of protein conformations, any changes in the atomic environment of a given nucleus may alter its observed chemical shift. Therefore, protein chemical shifts can be readily used to assess the structural quality of proteins through a comparison between experimental chemical shifts and those calculated by either QM or empirical models. In our previous study,[35] we successfully utilized the protein ^{1}H chemical shifts calculated

by the AF-QM/MM-PB method to discriminate the native structure of the Pin1 WW domain from the misfolded states. As demonstrated in that study, with the increase of the backbone RMSD with respect to the X-ray structure, the correlation of the calculated chemical shifts with experimental values declined accordingly, which shows that using ^{1}H chemical shifts as a tool to detect the native structure has a significant potential for protein structure validation.

Besides, the calculated chemical shifts can not only validate protein structures, but also detect the structural flaws for a given conformation. It is worth noting that the overall correlation of the calculated chemical shifts with the experiment based on the Pin1 WW domain NMR structures is not as good as that based on the X-ray structure. Fig. 1 shows the correlation between the experimental and AF-QM/MM-PB calculated ^{1}H chemical shifts of the Pin1 WW domain NMR structure. As can be seen from the figure, the correlation coefficient (R^2) is only 0.926.

As discussed in many other studies,[8] the accuracy of NMR structures highly depends on the quality of experimental constraints used in structural determination. Many errors may arise from mis-assignments of spectra, improper distance estimates, incomplete NOE restraints, spin-diffusion and dynamics. Therefore, the refinement of these questionable structures is highly desirable.[50] One can see from Fig. 1 that the calculated results based on the NMR structure show an obvious outlier: the HB2 atom of ASN21. For this atom, the calculated chemical shift is 2.07 ppm, while the experimental value is −0.64 ppm (BMRB entry: 4882). Moreover, calculated values for all the structures in the NMR ensemble give similar results. As the chemical shifts are very sensitive to the local structure of protein, such a large deviation from the experiment indicates significant structural flaws in the NMR structure.

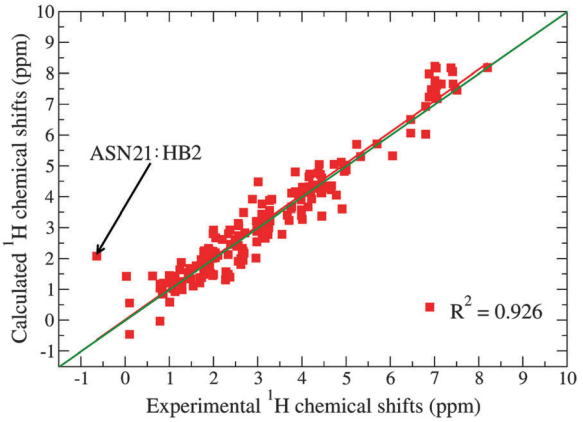

Fig. 1 Correlation between the experimental and AF-QM/MM-PB calculated ^{1}H NMR chemical shifts for the Pin1 WW domain NMR structure.

There are four main factors that may influence the chemical shifts of H atoms: paramagnetic effects, magnetic anisotropy around bonds, aromatic ring currents and electric field effects. Among these effects, only the ring current effect can cause very large upfield shifts for non-polar hydrogen atoms.[51,52] Therefore, we carefully checked the NMR structure, and found that the main source of errors may originate from the relative position of ASN21 and TRP6. The distance constraint from NOE data indicates that the separation between the HB2 atom of ASN21 (ASN21:HB2) and the HE3 atom of TRP6 (TRP6:HE3) is from 3.2 to 7.5 Å. As shown in Fig. 2, the indole ring of TRP6 in the NMR structure is far away from ASN21, which causes negligible ring current effects on the chemical shift of ASN21:HB2. Next, we take the side chain atoms of TRP6 and ASN21 as a model system to explore the influence of ring current effects from the indole ring on the chemical shift of ASN21:HB2 (see Fig. 3).

As shown in Fig. 3, when the distance between ASN21:HB2 and the indole ring (R) decreases, the calculated results show a significant upfield chemical shift. To be in accord with the experimentally observed chemical shift (−0.64 ppm), R must be around about 3.0 Å. Furthermore, there are also a few existing empirical models to approximate the influence of the ring

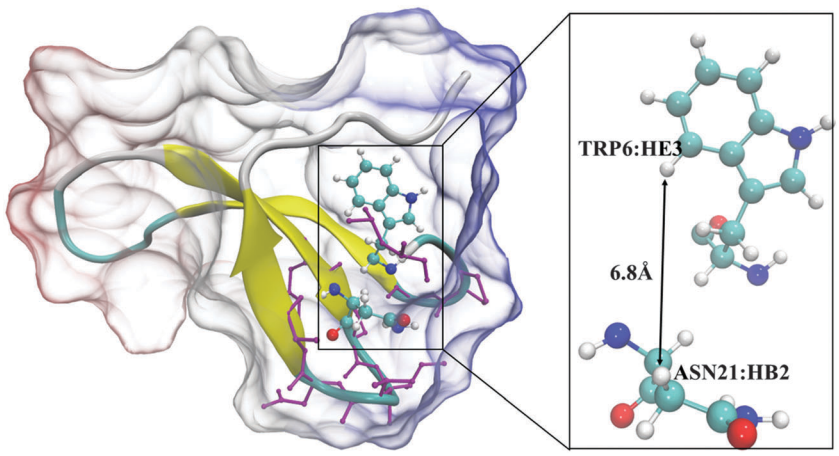

Fig. 2 The first Pin1 WW domain structure in the NMR ensemble. Residues of TRP6 and ASN21 are highlighted using ball and stick representation. In the AF-QM/MM-PB calculation, the core (ASN21) and buffer (TRP6 and residues denoted using purple sticks) regions are treated by QM methods. The rest of the protein and solvent effects are presented by point charges.

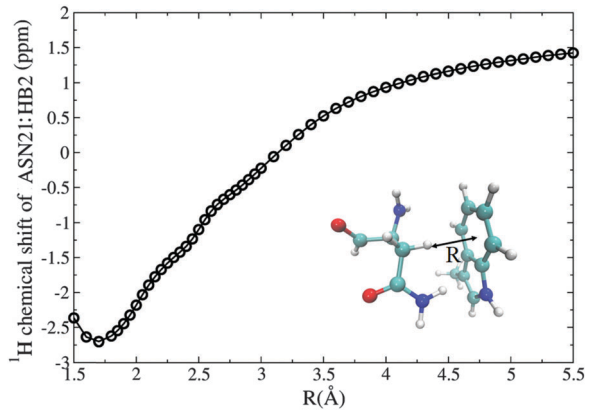

Fig. 3 NMR chemical shift of the ASN21:HB2 as a function of the distance between ASN21:HB2 and the center of the six-membered ring calculated at the B3LYP/6-31G** level.

current effect on the chemical shifts,[53,54] such as the Pople point dipole model[3,55,56] as follows:

$$\Delta\sigma_{\mathrm{ring}} = 10^6 \times \frac{ne^2a^2}{4\pi mc^2} \times \frac{1-3\cos^2\theta}{r^3} \quad (1)$$

where n is the number of circulating electrons, a is the radius of the ring (the carbon–carbon bond length of 1.39 Å is taken for the benzene ring), and r is the distance between the specified atom and the center of the ring. By substituting the experimental value of $\Delta\sigma_{\mathrm{ring}}$ for ASN21:HB2 in eqn (1), we obtained an r value of around 4.0 Å. However, this distance is as large as 8.57 Å in the NMR structure. In the experimental data, there are six NOE restraints between these two residues. Among them, the distance between TRP6:HE3 and ASN21:HB2 has a very loose range between 3.2 and 7.5 Å, which may cause the large separation between TRP6 and ASN21. Based on the aforementioned QM calculation of the chemical shift of ASN21:HB2, we modified this restraint to be between 3.2 and 5.0 Å and refined the protein structure using simulated annealing and MD simulation.

The root-mean-square deviation (RMSD) of protein backbone atoms and heavy atoms of TRP6 and ASN21 during MD simulation is shown in Fig. 4, respectively. For comparison, the X-ray structure (PDB id: 1PIN) is taken as the reference state. As can be seen from the figure, the overall secondary structure of the Pin1 WW domain was maintained during MD simulation. However, the TRP6 side-chain flipped after about 750 ps when using the Amber ff99SB force field. In contrast, the TRP6 side-chain flipped after 50 ps when the PPC charge model was employed. Furthermore, the RMSD of the heavy atoms of ASN21 and TRP6 decreased from 0.75 Å to around 0.5 Å after 3.2 ns using the Amber ff99SB force field. Notwithstanding, when the PPC charges were utilized in the structure refinement, the RMSD was further reduced to 0.25 Å, indicating that the refined structure by PPC is closer to the X-ray structure.

We select the final snapshots from both the AMBER and PPC trajectories, and calculated the ^{1}H chemical shifts using the AF-QM/MM method. The results are shown in Fig. 5 and Table 1.

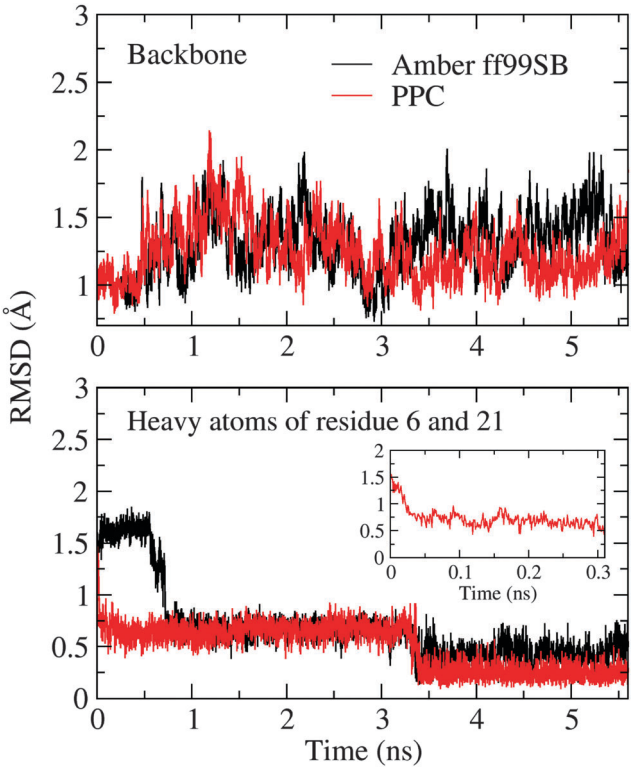

Fig. 4 RMSD of protein backbone atoms (upper panel) and heavy atoms of TRP6 and ASN21 (lower panel) during MD simulation. The X-ray structure is taken as the reference. The black and red lines show the results using the Amber ff99SB and PPC models, respectively.

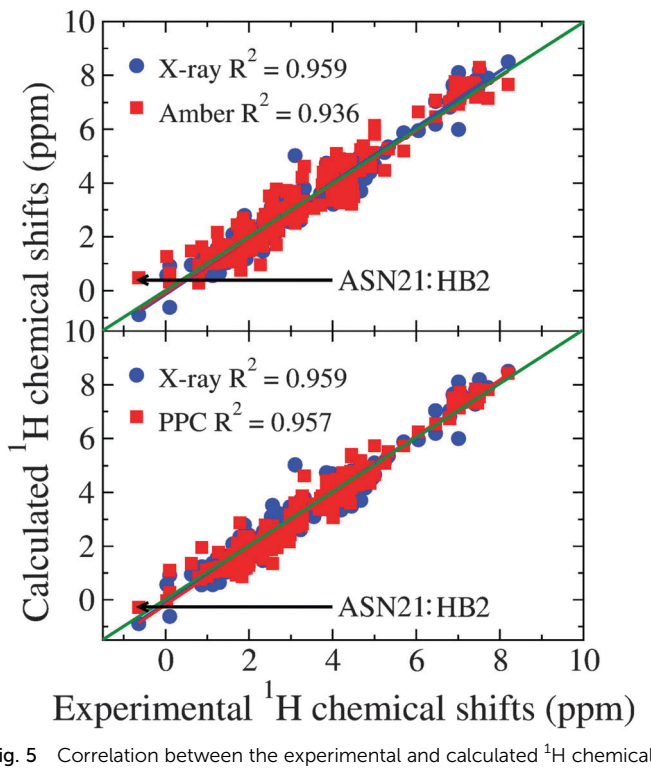

Fig. 5 Correlation between the experimental and calculated ^{1}H chemical shifts of the Pin1 WW domain based on both the X-ray and refined NMR structures. Blue circle: calculated ^{1}H chemical shifts of the X-ray structure. Red solid squares: calculated ^{1}H chemical shifts of the refined NMR structures (upper panel: Amber ff99SB force field; lower panel: PPC).

Table 1 Comparison of the calculated ASN21:HB2 chemical shifts of the Pin1 WW domain using the AF-QM/MM approach and four empirical methods together with the experimental value (in ppm)

	AF-QM/MM	SHIFTX2	PROSHIFT	SHIFTS4.1	SHIFTCALC	Exp.
NMR structure	2.07	2.45	2.82	2.87	2.93	−0.64
X-ray structure	−0.86	2.14	2.77	0.02	−0.04	
Refined structure (Amber ff99SB)	0.42	1.88	2.44	0.35	−0.18	
Refined structure (PPC)	−0.38	1.75	2.21	0.11	−0.22	

For comparison, the empirical models of SHIFTX2, PROSHIFT, SHIFTS4.1 and SHIFTCALC were also used to calculate the ASN21:HB2 chemical shift. This clearly shows that the AF-QM/MM-PB calculated results of ASN21:HB2 based on the refined NMR structure are in much better agreement with the experimental value than the original NMR structure, indicating that the relative position of ASN21 and TRP6 is more reasonable after refinement. It is also worth noting that the calculated result based on the PPC refinement (−0.38 ppm) is much closer to the experimental value (−0.64 ppm) than that from the Amber trajectory (0.42 ppm). Furthermore, the overall correlation (R^2) between calculated chemical shifts and experimental values based on the PPC refined structure is 0.957, which is very close to the result of 0.959 calculated based on the X-ray structure. In contrast, the correlation is 0.936 for the refined structure using the Amber ff99SB force field, indicating that the overall quality of the refined structure is improved when the electronic polarization effect is included in NMR structure refinement. We also compared the structural details of the final two snapshots (from Amber ff99SB and PPC MD simulations, respectively) as shown in Fig. 6. As one can see from that figure, the refined secondary structure of residues SER11 and GLY15 (highlighted in the black circle) using the Amber ff99SB force field has an anti-parallel β-sheet feature; however, this region is more flexible and presented as part of the loop structure in the X-ray structure. In contrast, the refined structure using the PPC model is in good agreement with the Pin1 WW domain X-ray structure. The hydrogen bond probabilities of several important hydrogen bonds during MD simulation are shown in Fig. S1 of the ESI.† We further plot the number of H-bonds as a function of simulation time as shown in Fig. S2 of the ESI.† One can see from the figure that more H-bonds were preserved in the PPC simulation than those in the Amber ff99SB simulation. These results underscore the importance of the electronic polarization effect in maintaining the correct secondary structure of proteins during NMR structure refinement.

As compared to the AF-QM/MM results, the difference in the ASN21:HB2 chemical shift between the NMR and X-ray structures predicted using both SHIFTX2 and PROSHIFT is very small as shown in Table 1. The chemical shift of ASN21:HB2 for the X-ray structure is 2.14 and 2.77 ppm, respectively, based on SHIFTX2 and PROSHIFT, which is significantly overestimated from the experimental value of −0.64 ppm. In contrast, SHIFTS4.1 and SHIFTCALC give much more reasonable predictions, as the chemical shifts of ASN21:HB2 for the X-ray structure are 0.02 and −0.04 ppm, respectively, based on SHIFTS4.1 and SHIFTCALC. The good performance of SHIFTS4.1 and SHIFTCALC shows that the empirical models they are using can correctly reflect the ring current effect for side chain proton atoms. The incorrect prediction of the chemical shift by other empirical methods may arise from the limited data for the side-chain atoms in the training set, which causes the unsuitable parameters in the knowledge-based empirical models. In a previous work of Ochsenfeld and co-workers,[57] it was also found that the chemical shifts predicted by most empirical methods were highly insensitive to protein structural changes, which renders their use for validating protein structures questionable. In contrast, the NMR chemical shifts calculated by *ab initio* methods have high sensitivity to the structural changes, and the QM methods do not rely on pre-defined empirical parameters. Therefore, quantum mechanics based methods such as AF-QM/MM are more general and accurate for protein side chain NMR chemical shift calculations. Moreover, the side chain atoms are usually flexible during MD simulations. Because the proton chemical shifts of side chains are very sensitive to the local chemical environment,

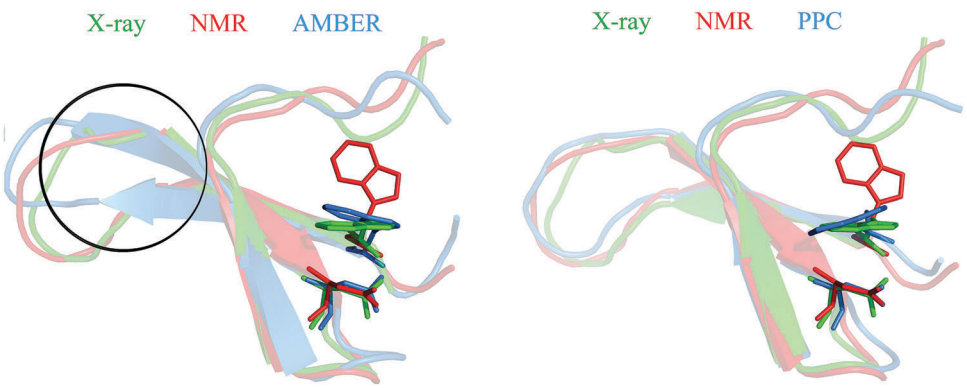

Fig. 6 Comparison of the X-ray (green) and NMR (red) structures of the Pin1 WW domain in the final refined conformation (blue) after MD simulation based on the Amber ff99SB (left) and PPC (right) charge models, respectively.

the AF-QM/MM method can be used for describing the dynamics of proteins *via* probing the change in those chemical shifts.

Conclusion

It is well known that not all NMR determined bio-molecular structures are of equally high quality. The refinement using the experimental restraints is highly desirable for those NMR structures with flaws. Since the chemical shifts are the most readily and accurately measurable NMR parameters, using chemical shifts as constraints in NMR structure validation and refinement has attracted a lot of attention recently. However, all the protocols that have been introduced so far require the reliability of predicting chemical shifts on given protein structures. Owing to the limitation of available experimental data, most of the widely used empirical models mainly focus on backbone chemical shifts, which are associated with protein secondary structures. Recent studies have demonstrated that there are quantitative relationships between the side-chain methyl groups and the tertiary structure of proteins.[3] Accurate prediction of side-chain chemical shifts may help to probe the side-chain packing in protein native structures. However, the relationship between the side chain chemical shifts and their specific conformation is complicated. So far, most of widely used sequence-based or structure-based empirical models do not always give a reliable prediction of the side chain chemical shifts. In this case, the QM method could be the best choice, because it does not rely on any empirical parameters and is very sensitive to the local structural changes.

In this study, the NMR structure of the Pin1 WW domain was validated and further refined based on the calculated side chain ^{1}H chemical shifts using the AF-QM/MM method. The AF-QM/MM approach has been proved to be computationally efficient and linear scaling with a small prefactor, and the calculated chemical shifts are accurate and reliable. Based on the calculated results, the experimental NOE restraints were modified in the structure refinement. The final refined structure is much closer to the X-ray structure than the original NMR structure. Moreover, the calculated ^{1}H chemical shifts based on the refined structure are in better agreement with the experimental values.

The study also demonstrates that the electronic polarization effect is of critical importance to maintaining the correct secondary structure of proteins in NMR structure refinement. The overall structure refined using the PPC model agrees better with the X-ray structure than the one refined using the non-polarizable Amber ff99SB force field. The computational protocol presented in this study can be further applied to other general bio-molecules and help to improve the accuracy in protein NMR structure determination.

Acknowledgements

This work was supported by the National Natural Science Foundation of China (Grants No. 10974054, 20933002 and 21303057) and Shanghai PuJiang program (09PJ1404000). X.H. is also supported by the Specialized Research Fund for the Doctoral Program of Higher Education (Grant No. 20130076120019) and the Fundamental Research Funds for the Central Universities. We thank the Supercomputer Center of East China Normal University for providing us computational time.

References

1 A. H. Kwan, M. Mobli, P. R. Gooley, G. F. King and J. P. Mackay, *FEBS J.*, 2011, **278**, 687–703.
2 P. Robustelli, K. A. Stafford and A. G. Palmer, III, *J. Am. Chem. Soc.*, 2012, **134**, 6365–6374.
3 A. B. Sahakyan, A. Cavalli, W. F. Vranken and M. Vendruscolo, *J. Phys. Chem. B*, 2012, **116**, 4754–4759.
4 M. Iwadate, T. Asakura and M. P. Williamson, *Eur. J. Biochem.*, 1998, **257**, 479–487.
5 D. S. Wishart, D. Arndt, M. Berjanskii, P. Tang, J. Zhou and G. Lin, *Nucleic Acids Res.*, 2008, **36**, W496–W502.
6 S. B. Nabuurs, C. A. E. M. Spronk, G. W. Vuister and G. Vriend, *PLoS Comput. Biol.*, 2006, **2**, 71–79.
7 J. Kuszewski, A. M. Gronenborn and G. M. Clore, *J. Magn. Reson., Ser. B*, 1995, **107**, 293–297.
8 J. Kuszewski, J. Qin, A. M. Gronenborn and G. M. Clore, *J. Magn. Reson., Ser. B*, 1995, **106**, 92–96.
9 G. M. Clore and A. M. Gronenborn, *Proc. Natl. Acad. Sci. U. S. A.*, 1998, **95**, 5891–5898.
10 B. J. Wylie, C. D. Schwieters, E. Oldfield and C. M. Rienstra, *J. Am. Chem. Soc.*, 2009, **131**, 985–992.
11 A. Cavalli, X. Salvatella, C. M. Dobson and M. Vendruscolo, *Proc. Natl. Acad. Sci. U. S. A.*, 2007, **104**, 9615–9620.
12 H.-b. Le, J. G. Pearson, A. C. de Dios and E. Oldfield, *J. Am. Chem. Soc.*, 1995, **117**, 3800–3807.
13 J. A. Vila, J. M. Aramini, P. Rossi, A. Kuzin, M. Su, J. Seetharaman, R. Xiao, L. Tong, G. T. Montelione and H. A. Scheraga, *Proc. Natl. Acad. Sci. U. S. A.*, 2008, **105**, 14389–14394.
14 Y. Shen, O. Lange, F. Delaglio, P. Rossi, J. M. Aramini, G. Liu, A. Eletsky, Y. Wu, K. K. Singarapu, A. Lemak, A. Ignatchenko, C. H. Arrowsmith, T. Szyperski, G. T. Montelione, D. Baker and A. Bax, *Proc. Natl. Acad. Sci. U. S. A.*, 2008, **105**, 4685–4690.
15 Y. Shen, R. Vernon, D. Baker and A. Bax, *J. Biomol. NMR*, 2009, **43**, 63–78.
16 J. Meiler and D. Baker, *Proc. Natl. Acad. Sci. U. S. A.*, 2003, **100**, 15404–15409.
17 O. A. Martin, Y. A. Arnautova, A. A. Icazatti, H. A. Scheraga and J. A. Vila, *Proc. Natl. Acad. Sci. U. S. A.*, 2013, **110**, 16826–16831.
18 Y. Shen and A. Bax, *J. Biomol. NMR*, 2012, **52**, 211–232.
19 M. C. Brothers, A. E. Nesbitt, M. J. Hallock, S. G. Rupasinghe, M. Tang, J. Harris, J. Baudry, M. A. Schuler and C. M. Rienstra, *J. Biomol. NMR*, 2012, **52**, 41–56.
20 Y. Shen, F. Delaglio, G. Cornilescu and A. Bax, *J. Biomol. NMR*, 2009, **44**, 213–223.
21 B. J. Wylie, L. J. Sperling, A. J. Nieuwkoop, W. T. Franks, E. Oldfield and C. M. Rienstra, *Proc. Natl. Acad. Sci. U. S. A.*, 2011, **108**, 16974–16979.

22 B. Han, Y. Liu, S. W. Ginzinger and D. S. Wishart, *J. Biomol. NMR*, 2011, **50**, 43–57.
23 J. Meiler, *J. Biomol. NMR*, 2003, **26**, 25–37.
24 K. Osapay and D. A. Case, *J. Am. Chem. Soc.*, 1991, **113**, 9436–9444.
25 D. Sitkoff and D. A. Case, *J. Am. Chem. Soc.*, 1997, **119**, 12262–12273.
26 X. P. Xu and D. A. Case, *J. Biomol. NMR*, 2001, **21**, 321–333.
27 M. P. Williamson and C. J. Craven, *J. Biomol. NMR*, 2009, **43**, 131–143.
28 M. P. Williamson and T. Asakura, *J. Magn. Reson., Ser. B*, 1993, **101**, 63–71.
29 M. P. Williamson, T. Asakura, E. Nakamura and M. Demura, *J. Biomol. NMR*, 1992, **2**, 83–98.
30 T. Asakura, K. Taoka, M. Demura and M. P. Williamson, *J. Biomol. NMR*, 1995, **6**, 227–236.
31 D. Sharma and K. Rajarathnam, *J. Biomol. NMR*, 2000, **18**, 165–171.
32 A. B. Sahakyan, W. F. Vranken, A. Cavalli and M. Vendruscolo, *Angew. Chem., Int. Ed.*, 2011, **50**, 9620–9623.
33 F. A. A. Mulder and M. Filatov, *Chem. Soc. Rev.*, 2010, **39**, 578–590.
34 X. He, B. Wang and K. M. Merz, Jr., *J. Phys. Chem. B*, 2009, **113**, 10380–10388.
35 T. Zhu, X. He and J. Z. H. Zhang, *Phys. Chem. Chem. Phys.*, 2012, **14**, 7837–7845.
36 T. Zhu, J. Z. H. Zhang and X. He, *J. Chem. Theory Comput.*, 2013, **9**, 2104–2114.
37 S. Tang and D. A. Case, *J. Biomol. NMR*, 2011, **51**, 303–312.
38 D. A. Case, *Curr. Opin. Chem. Biol.*, 2013, **23**, 172–176.
39 A. Frank, I. Onila, H. M. Moeller and T. E. Exner, *Proteins*, 2011, **79**, 2189–2202.
40 A. Frank, H. M. Möller and T. E. Exner, *J. Chem. Theory Comput.*, 2012, **8**, 1480–1492.
41 Q. Gao, S. Yokojima, D. G. Fedorov, K. Kitaura, M. Sakurai and S. Nakamura, *J. Chem. Theory Comput.*, 2010, **6**, 1428–1444.
42 M. K. Pandey and A. Ramamoorthy, *J. Phys. Chem. B*, 2013, **117**, 859–867.
43 T. Helgaker, M. Jaszuński and K. Ruud, *Chem. Rev.*, 1998, **99**, 293–352.
44 M. J. Frisch, G. W. Trucks, H. B. Schlegel, G. E. Scuseria, M. A. Robb, J. R. Cheeseman, J. A. J. Montgomery, T. Vreven, K. N. Kudin, J. C. Burant, J. M. Millam, S. S. Iyengar, J. Tomasi, V. Barone, B. Mennucci, M. Cossi, G. Scalmani, N. Rega, G. A. Petersson, H. Nakatsuji, M. Hada, M. Ehara, K. Toyota, R. Fukuda, J. Hasegawa, M. Ishida, T. Nakajima, Y. Honda, O. Kitao, H. Nakai, M. Klene, X. Li, J. E. Knox, H. P. Hratchian, J. B. Cross, V. Bakken, C. Adamao, J. Jaramillo, R. Gomperts, R. E. Stratmann, O. Yazyev, A. J. Austin, R. Cammi, C. Pomelli, J. W. Ochterski, P. Y. Ayala, K. Morokuma, G. A. Voth, P. Salvador, J. J. Dannenberg, V. G. Zakrzewski, S. Dapprich, A. D. Daniels, M. C. Strain, O. Farkas, D. K. Malick, A. D. Rabuck, K. Raghavachari, J. B. Foresman, J. V. Ortiz, Q. Cui, A. G. Baboul, S. Clifford, J. Cioslowski, B. B. Stefanov, G. Liu, A. Liashenko, P. Piskorz, I. Komaromi, R. L. Martin, D. J. Fox, T. Keith, M. A. Al-Laham, C. Y. Peng, A. Nanayakkara, M. Challacombe, P. M. W. Gill, B. Johnson, W. Chen, M. W. Wong, C. Gonzalez and J. A. Pople, *Gaussian 09, revision B.01*, Gaussian, Inc., Wallingford, CT, 2010.
45 R. Wintjens, J. M. Wieruszeski, H. Drobecq, P. Rousselot-Pailley, L. Buee, G. Lippens and I. Landrieu, *J. Biol. Chem.*, 2001, **276**, 25150–25156.
46 J. L. Markley, A. Bax, Y. Arata, C. W. Hilbers, R. Kaptein, B. D. Sykes, P. E. Wright and K. Wuthrich, *J. Mol. Biol.*, 1998, **280**, 933–952.
47 R. Salomon-Ferrer, D. A. Case and R. C. Walker, *Wiley Interdiscip. Rev.: Comput. Mol. Sci.*, 2013, **3**, 198–210.
48 L. L. Duan, Y. Mei, Q. G. Zhang and J. Z. H. Zhang, *J. Chem. Phys.*, 2009, **130**, 115102.
49 C. Ji, Y. Mei and J. Z. H. Zhang, *Biophys. J.*, 2008, **95**, 1080–1088.
50 N. M. Henriksen, D. R. Davis and T. E. Cheatham III, *J. Biomol. NMR*, 2012, **53**, 321–339.
51 A. S. Christensen, S. P. A. Sauer and J. H. Jensen, *J. Chem. Theory Comput.*, 2011, **7**, 2078–2084.
52 M. P. Williamson, *Prog. Nucl. Magn. Reson. Spectrosc.*, 2013, **73**, 1–16.
53 S. J. Perkins and K. Wuthrich, *Biochim. Biophys. Acta*, 1979, **576**, 409–423.
54 G. Moyna, R. J. Zauhar, H. J. Williams, R. J. Nachman and A. I. Scott, *J. Chem. Inf. Comput. Sci.*, 1998, **38**, 702–709.
55 A. B. Sahakyan and M. Vendruscolo, *J. Phys. Chem. B*, 2013, **117**, 1989–1998.
56 J. A. Pople, *J. Chem. Phys.*, 1956, **24**, 1111.
57 C. V. Sumowski, M. Hanni, S. Schweizer and C. Ochsenfeld, *J. Chem. Theory Comput.*, 2014, **10**, 122–133.